Low Reynolds Number Transport Properties of Axisymmetric Particles Employing Stick and Slip Boundary Conditions

Stuart A. Allison†

Department of Chemistry, Georgia State University, Atlanta, Georgia 30303

Received April 12, 1999; Revised Manuscript Received June 14, 1999

ABSTRACT: In this work, a numerical boundary element algorithm is described that can be applied to particles of arbitrary shape that are modeled as arrays of flat triangular plates. It is general enough to accommodate stick or slip boundary conditions as well as the presence of external forces on the surrounding fluid. The algorithm is used in the present work to study the transport of axisymmetric particles in the absence of external forces. Specifically, translational and rotational diffusion constants as well as the viscosity coefficient of ellipsoids (prolate and oblate), short rods, and toroids subject to stick and slip boundary conditions are reported. The transport properties of the corresponding "smooth" particles are estimated by carrying out numerical studies of several model structures and extrapolating to the limit of a model in which the number of plates goes to infinity. This is called the extrapolated shell model. Many of the transport properties are being reported for the first time. In cases where the transport properties are already known, the boundary element-extrapolated shell calculations are accurate to within a few percent.

Introduction

Scientists are frequently interested in determining various properties of molecules or microparticles such as their size, shape, and charge or how they interact with the surrounding solvent. From a variety of experiments, it is possible to measure various transport properties such as translational diffusion constants (from dynamic light scattering[1,2]), rotational diffusion constants (from fluorescence depolarization,[3,4] NMR,[4,5] electric birefringence[6−8] and dichroism,[9,10] and depolarized light scattering[5,11]), and intrinsic viscosity.[12] Also, the charge on a microparticle plays an important role on its transport in electric fields (electrophoresis[13,14]). Fluid mechanics has played a critical role in establishing concrete relationships between measurable transport properties and microscopic properties such as size, shape, and charge.[15−18] In a subdivision of fluid mechanics which is frequently referred to today as "microhydrodynamics",[18] the microparticle is modeled as a structure (not necessarily rigid), immersed in a continuous Newtonian fluid. The additional assumptions are usually made that the fluid is incompressible and that low Reynolds number conditions prevail.

It should be emphasized that fluid mechanics only carries us part of the way in relating transport properties to microscopic properties. Consider, for example, translational and rotational diffusion. From fluid mechanics, it is possible to determine the forces and torques on a model particle as it translates or rotates in a predefined way.[16−18] From these forces and torques, it is possible to determine the corresponding translational and rotational friction constants or, to be more precise, the friction tensors.[17,18] To make the link between friction and diffusion, it is necessary to apply statistical mechanics as was first done by Einstein almost a century ago.[19] Statistical mechanics can also be used to relate the excess bulk stress, or excess viscosity of a solution containing microparticles, to averages of the hydrodynamic stress and fluid flow around a single microparticle.[20] However, fluid mechanics must be used to determine these averages.

In the present work, we shall focus on the fluid flow around a single, solid particle. The solution shall be assumed dilute enough so that particle−particle interactions can be ignored. The boundary element method developed by Youngren and Acrivos[21] is used to calculate the forces, torques, and stresses around model particles. Well-established relationships are then used to determine translational and rotational diffusion constants as well as viscosity coefficients for ellipsoids (prolate and oblate), short rods, and toroids. In addition to the usual "stick" boundary condition, where the assumption is made that the fluid velocity matches the particle velocity at the fluid−particle interface, a parallel study using the "slip" boundary condition is carried out as well. In the slip boundary condition case, only the normal velocity component of fluid and particle match at the interface. In addition, however, there is no tangential component of the normal stress on the particle surface.[22] It has been known for some time that the rotational diffusion of certain small molecules, where hydrogen bonding with the solvent is known to be unimportant, are better explained by slip than by stick boundary conditions.[23−25] It has also been known for a long time that the hydrodynamic interaction between two identical spheres diverge as the two spheres come into contact.[17] Thus, the slip model could be relevant in such processes as diffusion-controlled reactions[26] and the hydrodynamic interaction of polymer segments that are in close proximity. In any event, there is a strong incentive to study the slip boundary condition case.

Hu and Zwanzig[22] computed slip rotational friction coefficients for prolate and oblate ellipsoids. Youngren and Acrivos have developed numerical boundary element (BE) procedures that are applicable to both the stick[21] and slip[24] cases. One advantage of the BE procedures[18,21,24] is that they can be applied to model particles of *arbitrary* shape. Furthermore, the BE

† E-mail: chesaa@panther.gsu.edu.

10.1021/ma990576c CCC: $18.00
Published on Web 07/22/1999

formalism is general enough that external forces on the solvent can be included, and this feature has been very useful in modeling the electrophoresis of particles of arbitrary shape and containing an arbitrary charge distribution within.[27,28] In this work, we shall describe a straightforward BE algorithm that works for both the stick and slip cases. Although external forces can be included in general, they are left out of the particular model systems studied in the present work.

Some of the results reported here are not new but are presented nonetheless to confirm the algorithm as well as evaluate the numerical results of others. These include the following: stick translational and rotational diffusion constants of ellipsoids, rods, and toroids; slip rotational diffusion constants of ellipsoids; stick viscosity coefficients of ellipsoids and rods; and the slip viscosity coefficient of spheres. Other results are, to the best of our knowledge, entirely new. These include slip translational diffusion constants of all particles (with the exception of a sphere); slip rotational diffusion constants of rods and toroids; stick viscosity coefficients of toroids; and slip viscosity coefficients of all structures with the exception of spheres.

Boundary Element Methodology

Let the particle be modeled as a rigid body enclosed by surface S_p, and let the volume exterior or interior to the particle be denoted by Ω or Ω_i, respectively. It shall be assumed that the particles are sufficiently dilute so that particle−particle interactions can be ignored. The solvent (in domain Ω) is represented as an incompressible Newtonian fluid with viscosity η_0. It is also assumed that the motion of the particle relative to the ambient fluid is small enough so that the fluid velocity is well described by the linearized Navier−Stokes and solvent incompressibility equations.

$$\eta_0\nabla^2\mathbf{v}(\mathbf{y}) - \nabla p(\mathbf{y}) = -\mathbf{s}(\mathbf{y}) \tag{1}$$

$$\nabla\cdot\mathbf{v}(\mathbf{y}) = 0 \tag{2}$$

where $\mathbf{v}(\mathbf{y})$ is the fluid velocity at field point $\mathbf{y}$ (in Ω), $p(\mathbf{y})$ is the fluid pressure, and $\mathbf{s}(\mathbf{y})$ denotes the external force per unit volume on the fluid at $\mathbf{y}$. The pressure is not explicitly needed to determine the transport properties of interest in this work. It does, however, contribute to the hydrodynamic stress forces acting on the particle surface to be discussed later. The external force term, $\mathbf{s}(\mathbf{y})$, can be of vital importance in certain transport phenomena such as electrophoresis or electroviscosity.[29−31] It is less important in modeling translational and rotational diffusion constants and viscosity coefficients of macromolecules, even if the macromolecules are charged.[14] Let $\mathbf{v}_\infty(\mathbf{y})$ denote the velocity the fluid would have at $\mathbf{y}$ if the particle were not present. In general, the particle perturbs the local fluid velocity (and pressure), but this perturbation falls off with distance so that $\mathbf{v} \rightarrow \mathbf{v}_\infty$ far from the particle. The velocity field (in Ω) is described by the boundary integral representation[15,18,21,24,27,31,32]

$$\mathbf{v}(\mathbf{y}) = \mathbf{v}_\infty(\mathbf{y}) + \mathbf{v}^{(0)}(\mathbf{y}) + \mathbf{v}^{(1)}(\mathbf{y}) + \mathbf{v}^{(2)}(\mathbf{y}) \tag{3}$$

where

$$\mathbf{v}^{(0)}(\mathbf{y}) = -\int_\Omega \boldsymbol{U}(\mathbf{x},\mathbf{y})\cdot\mathbf{s}(\mathbf{x})\, dV_x \tag{4}$$

$$\mathbf{v}^{(1)}(\mathbf{y}) = -\int_{S_p} \boldsymbol{U}(\mathbf{x},\mathbf{y})\cdot\mathbf{f}(\mathbf{x})\, dS_x \tag{5}$$

$$\mathbf{v}^{(2)}(\mathbf{y}) = \frac{3}{4\pi}\int_{S_p} \frac{\mathbf{r}[\mathbf{v}(\mathbf{x})\cdot\boldsymbol{R}(\mathbf{x},\mathbf{y})\cdot\mathbf{n}(\mathbf{x})]}{r^3}\, dS_x \tag{6}$$

$$\boldsymbol{U}(\mathbf{x},\mathbf{y}) = -\frac{1}{8\pi\eta_0 r}[\boldsymbol{I} + \boldsymbol{R}(\mathbf{x},\mathbf{y})] \tag{7}$$

$$[\boldsymbol{R}(\mathbf{x},\mathbf{y})]_{ij} = \frac{\mathbf{r}_i\mathbf{r}_j}{r^2} \tag{8}$$

$$\mathbf{r} = \mathbf{y} - \mathbf{x}; \quad r = |\mathbf{r}| \tag{9}$$

In eq 7, $\mathbf{I}$ denotes the 3 × 3 identity matrix, $\mathbf{f}(\mathbf{x})$ appearing in eq 5 represents the hydrodynamic stress force per unit area at point $\mathbf{x}$ on the particle surface, and $\mathbf{n}(\mathbf{x})$ appearing in eq 6 represents the outward unit normal (into the fluid) of S_p at $\mathbf{x}$. It should be emphasized that eq 3 only yields the fluid velocity *outside* of S_p (in Ω). Indeed, if $\mathbf{y}$ is taken as an interior point (in Ω_i), the sum of terms on the right-hand side (rhs) gives $\mathbf{0}$. Also, for a point $\mathbf{y}_s$ on S_p

$$\frac{1}{2}\mathbf{v}(\mathbf{y}_s) = \mathbf{v}_\infty(\mathbf{y}_s) + \mathbf{v}^{(0)}(\mathbf{y}_s) + \mathbf{v}^{(1)}(\mathbf{y}_s) + \mathbf{v}^{(2)}(\mathbf{y}_s) \tag{10}$$

This arises as a consequence of a discontinuous jump in the "double-layer" term, $\mathbf{v}^{(2)}(\mathbf{y})$, across S_p.

At this point, it is important to distinguish between the two hydrodynamic boundary condition cases that are considered in this work. In the case of stick boundary conditions (bc's), it is assumed that the fluid velocity and particle velocity are equal on S_p. Suppose the particle translates with linear velocity $\mathbf{u}$ and rotates with angular velocity $\boldsymbol{\omega}$ about some point chosen to define the origin of some convenient particle-fixed reference frame. At point $\mathbf{y}_s$ on the particle surface

$$\mathbf{v}(\mathbf{y}_s) = \mathbf{u} + \boldsymbol{\omega}x\mathbf{y}_s \tag{11}$$

If the fluid exhibits rigid body motion on S_p, it can be shown that $\mathbf{v}^{(2)}(\mathbf{y})$ equals $\mathbf{0}$ if $\mathbf{y}$ is exterior to the surface and $-\mathbf{v}(\mathbf{y}_s)/2$ if $\mathbf{y}_s$ is on S_p (see ref 32 as well as the Appendix of ref 33). Using this property of the double-layer term which is valid when stick boundary conditions hold, it is permissible to write

$$\mathbf{v}(\mathbf{y}) = \mathbf{v}_\infty(\mathbf{y}) + \mathbf{v}^{(0)}(\mathbf{y}) + \mathbf{v}^{(1)}(\mathbf{y}) \tag{12}$$

where eq 12 is now valid both in Ω and on S_p. It should be emphasized that the double-layer term does not vanish on S_p, but its contribution has been transferred from the rhs to the left-hand side of the equation. Thus, in numerical solutions of flow around rigid particles where stick boundary conditions are employed, the double-layer term can be ignored.

In the case of slip boundary conditions, the assumption is made that only the normal component of the fluid velocity matches the particle velocity on S_p,

$$(\mathbf{u} + \boldsymbol{\omega}x\mathbf{y}_s)\cdot\mathbf{n}(\mathbf{y}_s) = \mathbf{v}(\mathbf{y}_s)\cdot\mathbf{n}(\mathbf{y}_s) \tag{13}$$

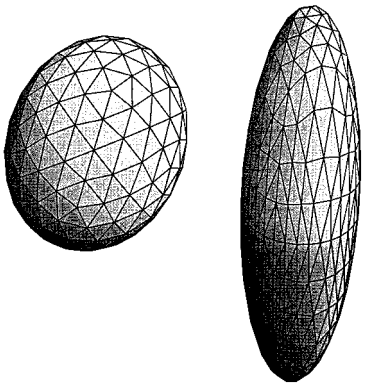

Figure 1. Oblate and prolate ellipsoid models. The ratio b/a is 0.75 and 4.0, respectively, and the number of platelets, N, making up the model is 320 (oblate) and 512 (prolate), respectively.

Furthermore, the assumption is made that the hydrodynamic stress forces are normal to the particle surface,

$$\mathbf{f}(\mathbf{y}_s) = \mathbf{n}(\mathbf{y}_s)[\mathbf{n}(\mathbf{y}_s)\cdot\mathbf{f}(\mathbf{y}_s)] \tag{14}$$

In the slip case, the double-layer term appearing in eqs 3 and 10 cannot be ignored or, as in the case of a point on the particle surface *with stick boundary conditions*, be absorbed into the left-hand side of eq 10. Nonetheless, it is still possible to numerically solve the transport problem with either stick or slip boundary conditions. In the absence of $\mathbf{v}_\infty$ and $\mathbf{v}^{(0)}$ terms, BE algorithms were developed over 20 years ago for both the stick[21] and slip[24] boundary condition cases. In what follows, we describe a general, but straightforward, algorithm that readily accommodates both.

The actual surface, S_p, is approximated as an interconnected set of N flat triangular platelets. Representative examples for oblate and prolate ellipsoidal particles are shown in Figure 1. The approximation is made that physical quantities such as fluid velocity, $\mathbf{v}$, pressure, p, and hydrodynamic stress force per unit area, $\mathbf{f}$, are constant over a particular platelet but can vary from one platelet to another. Let $\mathbf{v}_i$ denote the fluid velocity on platelet i (the centroid position vector is denoted $\mathbf{y}_i$). Given the discretization approximation discussed above, eq 10 can be written

$$\frac{1}{2}\mathbf{v}_i = \mathbf{v}_{\infty i} + \mathbf{v}_i^{(0)} + \sum_{j=1}^{N}(\boldsymbol{G}_{ij}\cdot\mathbf{f}_j + \boldsymbol{D}_{ij}\cdot\mathbf{v}_f) \tag{15}$$

where

$$\mathbf{v}_i^{(0)} = -\int_\Omega \boldsymbol{U}(\mathbf{x},\mathbf{y}_i)\cdot\mathbf{s}(\mathbf{x})\,\mathrm{d}V_x \tag{16a}$$

$$\boldsymbol{G}_{ij} = -\int_{S_j} \boldsymbol{U}(\mathbf{x},\mathbf{y}_i)\,\mathrm{d}S_x \tag{16b}$$

$$\boldsymbol{D}_{ij} = +\frac{3}{4\pi}\int_{S_j}\frac{\mathbf{r}[\boldsymbol{R}(\mathbf{x},\mathbf{y}_i)\cdot\mathbf{n}(\mathbf{x})]}{r^3}\,\mathrm{d}S_x \tag{16c}$$

and S_j denotes the surface of platelet j. The unknowns in eq 15 are the components of $\mathbf{v}_i$ and $\mathbf{f}_i$. It is assumed that the external forces, $\mathbf{s}(\mathbf{x})$, are known to some level approximation in advance so that the $\mathbf{v}_i^{(0)}$ are known.[27,28] For a particular model structure, it is straightforward to numerically compute the $\mathbf{G}_{ij}$ and $\mathbf{D}_{ij}$ matrices. There are N^2 3×3 $\mathbf{G}_{ij}$ and $\mathbf{D}_{ij}$ matrices involving surface integrals that are evaluated numerically using well-established procedures.[27] Although a considerable amount of computation time is involved in determining these matrices, it should be emphasized that they only need to be computed once for a given structure. Equation 15 represents $3N$ equations in $6N$ unknowns. It is convenient to write this in compact matrix form as

$$\frac{1}{2}\mathbf{v} = \mathbf{v}_\infty + \mathbf{v}^{(0)} + \boldsymbol{G}\cdot\mathbf{f} + \boldsymbol{D}\cdot\mathbf{v} \tag{17}$$

where the lower case symbols represent $3N \times 1$ column vectors and the upper case symbols represent $3N \times 3N$ matrices. The fourth through sixth elements of the column vector, $\mathbf{f}$, represent the x through z components of $\mathbf{f}_2$, for example. The $3N \times 3N$ $\mathbf{G}$ and $\mathbf{D}$ supermatrices are made up of the N^2 3×3 $\mathbf{G}_{ij}$ and $\mathbf{D}_{ij}$ matrices with the ijth submatrix of $\mathbf{G}$ (or $\mathbf{D}$) corresponding to $\mathbf{G}_{ij}$ (or $\mathbf{D}_{ij}$). In this form, it is particularly straightforward to solve eq 17 for the stick case since $\mathbf{D}\cdot\mathbf{v} \rightarrow -\mathbf{v}/2$. Defining $\mathbf{G}^{-1}$ as the inverse of $\mathbf{G}$, eq 17 can be inverted to give

$$\mathbf{f} = \boldsymbol{G}^{-1}\cdot(\mathbf{v} - \mathbf{v}_\infty - \mathbf{v}^{(0)}) \tag{18}$$

In the typical Resistance problem,[16−18] the particle velocity and ambient fluid velocity are specified and the stress forces computed. Once these are known, transport properties such as translational and rotational diffusion constants as well as viscosity coefficients can be determined as described in the next subsection of this paper. Thus, the quantities on the rhs side of eq 19 are known. With the widespread availability of mathematical software such as IMSL,[34] the inversion of large matrices has become routine. Thus, eq 18 is readily solved, and with it, the stresses for the stick boundary condition case are determined.

For the slip condition, it is convenient to write

$$\mathbf{v} = \mathbf{v}_N + \mathbf{v}_T \tag{19}$$

where $\mathbf{v}_N$ is the normal component of the $3N \times 1$ general velocity vector at the particle surface (which is known from the boundary conditions) and $\mathbf{v}_T$ is the corresponding tangential component, which is not known. Then eq 17 can be written

$$\left(\frac{1}{2}\boldsymbol{E} - \boldsymbol{D}\right)\cdot\mathbf{v}_T - \mathbf{a} = \boldsymbol{G}\cdot\mathbf{f} \tag{20}$$

where

$$\mathbf{a} = \frac{1}{2}\mathbf{v}_N - \boldsymbol{D}\cdot\mathbf{v}_N - \mathbf{v}_\infty \tag{21}$$

and $\mathbf{E}$ is the $3N \times 3N$ identity matrix. It is also convenient to define the $3N \times 3N$ supermatrix, $\mathbf{N}$, made up N^2 3×3 matrices, $\mathbf{N}_{ij}$. For i and j different, $\mathbf{N}_{ij} = \mathbf{0}$. Also, $(\mathbf{N}_{ii})_{\alpha\beta} = n_{i\alpha}n_{i\beta}$ where $n_{i\alpha}$ is the α-component ($\alpha = x, y,$ or z) of the outward normal of platelet i. There are $6N$ unknowns in eq 20 but only $3N$ equations. From the boundary condition that the stress forces are normal to the particle surface (eq 14), we also have the $3N$ equations

$$(\boldsymbol{E} - \boldsymbol{N})\cdot\mathbf{f} = \mathbf{0} \tag{22}$$

To solve eq 20 for both $\mathbf{f}$ and $\mathbf{v}_T$, we have found the following iterative method of solution to be both straightforward and useful. Start with some initial estimate of

$\mathbf{v}_T$; call it $\mathbf{v}_T^0$. (Set $\mathbf{v}_T^0 = \mathbf{0}$, for example.) Then eq 20 can be inverted to get an estimate of $\mathbf{f}$; call it $\mathbf{f}^{est}$:

$$\mathbf{f}^{est} = \boldsymbol{G}^{-1}\cdot\left[\left(\frac{1}{2}\boldsymbol{E} - \boldsymbol{D}\right)\cdot\mathbf{v}_T^0 - \mathbf{a}\right] \tag{23}$$

To ensure that our estimate satisfies eq 22, premultiply eq 23 by $\mathbf{N}$ to obtain estimate $\mathbf{f}^1$

$$\mathbf{f}^1 = \boldsymbol{N}\cdot\boldsymbol{G}^{-1}\cdot\left[\left(\frac{1}{2}\boldsymbol{E} - \boldsymbol{D}\right)\cdot\mathbf{v}_T^0 - \mathbf{a}\right] \tag{24}$$

Now because we have applied $\mathbf{N}$ to $\mathbf{f}^{est}$, $\mathbf{f}^1$ is no longer a solution of eq 23 with $\mathbf{v}_T$ approximated with $\mathbf{v}_T^0$. We can use $\mathbf{f}^1$ to get a better estimate $\mathbf{v}_T$. Solving eq 20 for $\mathbf{v}_T{}^{est}$

$$\mathbf{v}_T^{est} = \left(\frac{1}{2}\boldsymbol{E} - \boldsymbol{D}\right)^{-1}\cdot(\boldsymbol{G}\cdot\mathbf{f}^1 + \mathbf{a}) \tag{25}$$

This can then be corrected to remove the normal component by premultiplying eq 25 by $(\mathbf{E} - \mathbf{N})$

$$\mathbf{v}_T^1 = (\boldsymbol{E} - \boldsymbol{N})\cdot\left(\frac{1}{2}\boldsymbol{E} - \boldsymbol{D}\right)^{-1}\cdot(\boldsymbol{G}\cdot\mathbf{f}^1 + \mathbf{a}) \tag{26}$$

Successive applications of eqs 24 and 26 using improved estimates are then performed until $\mathbf{f}$ and $\mathbf{v}_T$ converge. It should be emphasized that all $3N \times 3N$ matrices appearing in eqs 24 and 26 as well as the $3N \times 1$ $\mathbf{a}$ vector only need to be computed once for a given structure. This, however, is the most time-consuming part of the calculation, and the iterative phase of the calculation proceeds relatively quickly.

In some cases, this iterative scheme does not lead to convergence. However, a straightforward procedure of underrelaxation usually does work. Let $\mathbf{f}^j$ denote the jth estimate of $\mathbf{f}$, and let $\mathbf{f}^*$ a tentative updated estimate using the scheme described in the previous paragraph. The actual new estimate, $\mathbf{f}^{j+1}$, is taken to be

$$\mathbf{f}^{j+1} = \lambda(\mathbf{f}^* - \mathbf{f}^j) + \mathbf{f}^j \tag{27}$$

where λ is the relaxation parameter taken to be between 0 and 1 in the case of underrelaxation. An entirely analogous approach can also be applied to $\mathbf{v}_T$. On occasion, the stresses or tangential velocities may fail to converge even if λ is set close to zero. In this case the structure itself may have to be replaced by one made up of a larger number of platelets so that the approximation of constant stress over a single platelet is more readily satisfied. It is likely that instability in convergence, which forces one to underrelax, is related to (a) a poor initial choice in $\mathbf{v}_T^0$, (b) approximations associated with discretizing the particle surface, or (c) using triangular instead of more general quadrilateral surface elements. In a broader sense, overall accuracy may be limited by the ill-conditioned nature of methods that involve single-layer integral equations.[18] Nonetheless, we shall show that the present methodolgy yields transport properties that are accurate to within a few percent in cases where those transport properties are already known.

Relationship to Transport

Once the stresses and surface velocities have been numerically determined as described in the previous section, it is possible to relate these to transport coefficients. The particles considered in this work (ellipsoids, rods, and toroids) are axisymmetric, and there is no coupling between translational and rotational motion. Also, the centers of diffusion and friction[18] correspond to the particle "center of mass" (CM), although it should be emphasized that this is not true for structures in general. It shall also be assumed that there are no external forces present ($\mathbf{s}(\mathbf{x}) = \mathbf{0}$). The total hydrodynamic force on the particle, $\mathbf{h}$, and the corresponding torque, $\mathbf{k}$, are given by

$$\mathbf{h} = -\sum_{j=1}^{N}\mathbf{f}_j A_j \tag{28}$$

$$\mathbf{k} = -\sum_{j=1}^{N}(\mathbf{y}_j \times \mathbf{f}_j)A_j \tag{29}$$

where $\mathbf{f}_j$ is the stress force per unit area on platelet j, A_j is the platelet area, and $\mathbf{y}_j$ is the centroid of platelet j relative to the particle "center of mass". The 3 (or "z") direction is chosen to correspond to the axis of symmetry of the particle. If the particle translates along the z-direction with speed u, the parallel translational friction coefficient, $\zeta_{t\parallel}$, is simply $-h_3/u$. The perpendicular translational friction coefficient, $\zeta_{t\perp}$, is obtained in a similar manner by translating the particle in the 1 or 2 direction. The rotational friction coefficients, $\zeta_{r\parallel}$ and $\zeta_{r\perp}$, are obtained by rotating the particle with angular velocity ω, computing the torque according to eq 29 and setting $\zeta_{ri} = -k_i/\omega$ where $i = 3$ gives the parallel and $i = 1$ or 2 the perpendicular component. The corresponding diffusion constants, D_{ti} and D_{ri}, are related to the friction coefficients by[35]

$$D_{ti} = \frac{k_B T}{\zeta_{ti}} \tag{30}$$

where k_B is Boltzmann's constant and T is absolute temperature. A similar relationship holds for D_{ri}. In measurements of translational diffusion, one typically measures an orientationally averaged diffusion constant, D_t, which is given by

$$D_t = \frac{D_{t\parallel} + 2D_{t\perp}}{3} \tag{31}$$

In the present work, all diffusional transport data shall be reported in terms of the dimensionless quantities

$$X_{ti} = \frac{D_{ti}}{D_t^0} \tag{32a}$$

$$X_{ti} = \frac{D_{ri}}{D_r^0} \tag{32b}$$

where D_t^0 is the stick translational diffusion constant of a sphere having the same volume as that of the structure being modeled and D_r^0 is the corresponding stick rotational diffusion constant.

Let η_0 denote the solvent viscosity in the absence of particles and η the viscosity when the number concentration of particles is c. It is assumed the solution

contains a monodisperse suspension of particles. The dimensionless viscosity coefficient is defined

$$\xi = \lim_{c \to 0} \frac{1}{cV_p}\left(\frac{\eta}{\eta_0} - 1\right) \tag{33}$$

where V_p is the particle volume. For spheres, $\xi = {}^5/_2$ for stick bc's[19] and $\xi = 1$ for slip bc's.[36] Its value is also well-known for prolate and oblate ellipsoids[37−39] with stick bc's and equations, tables, and graphs can be found in a number of popular texts.[40,41] For the present work, a relationship due to Batchelor[20] and extended by Russel[42] to include external forces is very useful. In terms of ξ, we can write

$$\xi = -\frac{1}{\gamma\eta_0 V_p}[\langle\int_{S_p}[\mathbf{w}_1\mathbf{y}_2 + \eta_0(\mathbf{v}_1\mathbf{n}_2 + \mathbf{v}_2\mathbf{n}_1)]\,dS_y\rangle + \langle\int_\Omega \mathbf{s}_1\mathbf{y}_2\,dV_y\rangle] \tag{34}$$

where γ is the shear gradient, 1 and 2 indices indicate x and y components in a laboratory (not body-fixed) frame of reference, S_p denotes the particle surface, Ω is the fluid domain exterior to the particle, and other quantities have been defined previously in this subsection. The brackets, $\langle\ \rangle$, indicate an ensemble average over all possible orientations of the particle. Here, it shall be assumed that the shear gradient is low enough and that the Brownian motion of the particles is great enough that all particle orientations are equally probable to a good approximation. In this case, it is possible to carry out calculations of a particle in five different elementary shear configurations ($m = 1-5$) and compute ξ by an averaging procedure described previously.[31] Basically, the different shear configurations are sampled as the orientation of the particle varies, and a particular orientation can be described in terms of a linear superposition of the five elementary shear configurations. (Keep in mind that a pure shear field can be characterized by a symmetric, traceless, second-rank Cartesian tensor. Hence, specifying five of the nine components uniquely defines the tensor. This explains why there are five independent elementary shear fields.) For a detailed description of the averaging procedure, see Appendix A of ref 31. It is possible to write

$$\xi = \frac{1}{5}(\xi_{12}^{(1)} + \xi_{13}^{(2)} + \xi_{23}^{(3)}) + \frac{1}{15}(\xi_{11}^{(4)} + \xi_{33}^{(4)} - 2\xi_{22}^{(4)} + \xi_{11}^{(5)} + \xi_{22}^{(5)} - 2\xi_{33}^{(5)}) \tag{35}$$

where

$$\xi_{\alpha\beta}^{(m)} = -\frac{1}{\eta_0\gamma V_p}(\sum_{j=1}^{N}[\mathbf{r}_j\cdot\boldsymbol{P}_{\alpha\beta}\cdot\mathbf{f}_j^{(m)} + 2\eta_0\mathbf{n}_j\cdot P_{\alpha\beta}\cdot\mathbf{v}_j^{(m)}] + \sum_k \mathbf{r}_j\cdot\boldsymbol{P}_{\alpha\beta}\cdot\mathbf{s}_k^{(m)}) \tag{36a}$$

$$\boldsymbol{P}_{\alpha\beta} = \frac{1}{2}(\mathbf{e}_\alpha\mathbf{e}_\beta + \mathbf{e}_\beta\mathbf{e}_\alpha) \tag{36b}$$

where $\mathbf{r}_j$ is the position of platelet j in a particle frame of reference with the origin chosen to correspond to the particle center of rotation (center of mass for axisymmetric particles), the "m" superscript denotes the quantity in the mth shear configuration, $\mathbf{n}_j$ denotes the outward surface normal of platelet j, and the sum over k is over all volume elements surrounding the particle.

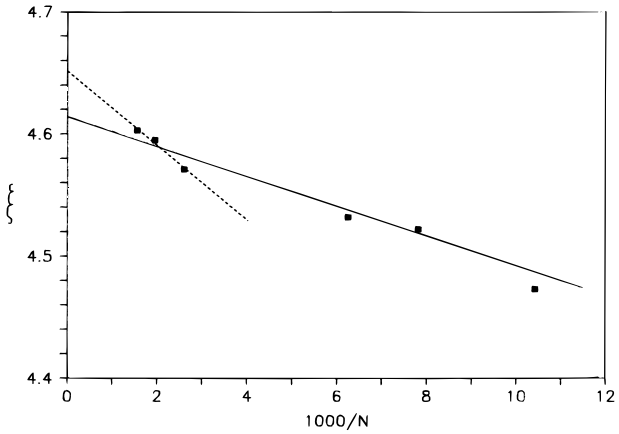

Figure 2. Plot of ξ versus $N - 1$ for a 4:1 prolate ellipsoid (stick bc's). The values extracted from BE calculations are denoted by squares. The dashed line represents linear least-squares fit of the three BE values with largest N (384, 512, and 640) whereas the solid lin represents the fit to all six data points.

In the absence of external forces the "sum over k" term does not contribute. Finally, $\mathbf{e}_\alpha$ is a unit vector in direction α. Equation 36a is very similar to eq A17 of ref 31, but the second term on the rhs is new. It does not contribute when stick boundary conditions hold, since the particle is stationary in the particle frame of reference, but it does contribute under slip boundary conditions. The averaging procedure employed in deriving eq 36a was shown previously to reproduce quite accurately the viscosity coefficient of prolate ellipsoids.[31] Furthermore, in Appendix B of ref 31, it was shown to be equivalent to a general expression derived by Garcia de la Torre and Bloomfield for an arbitrary object modeled as an array of beads.[43] In summary, the viscosity coefficient is determined by first determining **f** and **v** for the particle placed in five different elementary shear configurations (see Appendix A of ref 31), computing the $\xi_{\alpha\beta}^{(m)}$ following eqs 36a−b and then using these in eq 35.

Model Structures and Extrapolated Shell

Shown in Figure 1 are representative examples of oblate and prolate ellipsoid models used in this work. All structures consist of from $N = 80$ to 800 flat triangular platelets interconnected to form a closed surface. As discussed previously, the approximation is made that physical quantities such as the stress force and surface fluid velocities are constant over each platelet. Since these quantities actually vary continuously over the structure, those models made up of the most platelets are expected to yield the most accurate transport properties. On the other hand, computational constraints limit one to structures of about $N = 1000$ or fewer. In an attempt to deal with this problem, several different models are investigated for each structure in which the number of platelets is varied. Then, a linear least-squares fit of each transport property versus $1/N$ is carried out, and the transport property is approximated by the $1/N \to 0$ limit. This shall be referred to as the "extrapolated shell" limit. The same procedure has long been used in models where the structure is represented as an array of beads.[44,45] Figure 2 illustrates the extrapolated shell approach as applied to the case of the stick viscosity coefficient of a 4:1 prolate ellipsoid (major axis/minor axis = 4). Plotted is

Table 1. Transport Properties of Ellipsoids (Stick)

b/a	$X_{t\|\|}$	$X_{t\perp}$	X_t	$X_{r\|\|}$	$X_{r\perp}$	ξ
0.10	0.548	0.760	0.689	0.210	0.237	7.92
			(0.686)	(0.209)	(0.232)	(8.06)
0.25	0.730	0.925	0.860	0.445	0.549	4.02
			(0.858)	(0.444)	(0.543)	(4.06)
0.50	0.879	1.002	0.962	0.710	0.889	2.84
			(0.960)	(0.709)	(0.884)	(2.85)
0.75	0.957	1.012	0.994	0.882	1.013	2.55
			(0.993)	(0.881)	(1.010)	
1.0	1.001	1.001	1.001	1.002	1.002	2.49
			(1.000)	(1.000)	(1.000)	(2.50)
2.0	0.913	1.046	0.958	0.665	1.24	2.91
			(0.958)	(0.664)	(1.24)	(2.91)
3.0	0.835	1.026	0.899	0.428	1.34	3.68
			(0.899)	(0.427)	(1.34)	(3.68)
4.0	0.773	0.993	0.846	0.295	1.39	4.65
			(0.846)	(0.294)	(1.39)	(4.66)
5.0	0.723	0.958	0.801	0.216	1.43	5.78
			(0.800)	(0.215)	(1.42)	(5.81)
6.0	0.681	0.924	0.762	0.166	1.45	7.07
			(0.761)	(0.165)	(1.44)	(7.10)
8.0	0.617	0.865	0.700	0.107	1.49	10.04
			(0.698)	(0.106)	(1.46)	(10.10)
10.0	0.568	0.815	0.650	0.075	1.51	13.52
			(0.648)	(0.075)	(1.47)	(13.63)

Table 2. Transport Properties of Ellipsoids (Slip)

b/a	$X_{t\|\|}$	$X_{t\perp}$	X_t	$X_{r\perp}$	ξ
0.10	0.560	3.83	2.74	0.260	1.70
				(0.253)	
0.25	0.789	2.11	1.67	0.837	1.44
				(0.816)	
0.50	1.06	1.77	1.53	3.42	1.13
				(3.39)	
0.75	1.29	1.62	1.51	19.2	1.02
				(19.4)	
1.0	1.50	1.50	1.50		1.00
			(1.50)	(∞)	(1.00)
2.0	1.22	2.28	1.57	2.74	1.19
				(2.77)	
3.0	1.07	3.02	1.72	0.925	1.58
4.0	1.01	3.90	1.97	0.502	2.06
				(0.504)	
5.0	1.02	4.97	2.34	0.326	2.71
				(0.326)	
6.0	1.09	6.16	2.78	0.232	3.42
8.0	1.39	9.53	4.10	0.139	5.15
10.0	1.83	12.8	5.48	0.094	7.06
				(0.094)	

ξ versus $1/N$, and the solid and dashed lines represent different linear least-squares fits to the data (denoted by squares). The number of platelets varies from 96 to 640 in this case. Unfortunately, the data do not lie on a straight line, and this affects the accuracy of the extrapolated shell value. The solid and dashed lines illustrate this where all data points are used in one fit (solid line), but only the ξ values for the three largest N models (384, 512, and 640) are used in the second (dashed line). The actual ξ is 4.663 (taken directly from Tables 10−2 of ref 40). The extrapolated shell values from Figure 2 are 4.616 (solid line) and 4.652 (dashed line), which are lower than the actual values by 1.0% and 0.2%, respectively. This example illustrates the limitation of the BE approach in calculating transport properties. Because of the discrete nature of the models, the resultant transport properties are approximate, and nonlinearity in the extrapolated shell approach as implemented in the present work limits accuracy to within a few percent of the actual value. It should also be pointed out, however, that the same difficulty is also encountered in the "bead methods"[46] which have been extensively used in studying transport of complex structures with stick boundary conditions.[47]

In the following sections, the extrapolated shell approach as described above is used to estimate transport properties. A number of structures are constructed and studied in which N varies over a fairly wide range. By using a wide range of N values, one minimizes the uncertainty of making a long extrapolation from data that is relatively closely spaced. It should also be pointed out that the transport properties will depend not only on N but on the details of the structures as well.[28] In the present work, we have attempted to design structures made up of platelets that are not too long and slender since for such structures, the assumption of constant surface stress or surface velocity may be a poor one.

Results

Ellipsoids. The transport properties of prolate and oblate ellipsoids have been extensively studied in the past and provide the best check of the boundary element (BE) algorithm with regard to both stick and slip boundary conditions. Table 1 summarizes the ellipsoid results for stick boundary conditions. The volume of the ellipsoid is $4\pi a^2 b/3$ where "a" is the major axis for a oblate ellipsoid and the minor axis for a prolate and "b" is the remaining axis. The ratio b/a is less than one for a oblate and greater than one for a prolate ellipsoid. The first line for each b/a value represents the extrapolated shell value extracted from the BE calculation. The entries appearing in the following line and in parentheses represent exact values. For translation and rotation, the Perrin equations[48] as summarized in ref 41 are used. The viscosity factors, ξ, are taken directly from Table 10-2 of ref 41 and are based on earlier work.[37−39] The case of a sphere ($b/a = 1$) comes from earlier work still by Einstein.[19]

The corresponding results for slip boundary conditions are shown in Table 2. In this case, there are fewer known transport properties to compare the BE values with. Past work has been confined almost entirely to rotation perpendicular to the axis of symmetry,[22,24] although the slip translation of a sphere has been known for a long time.[49] For the slip case, the extrapolated shell value of $X_{r\perp}$ agrees with past work to an accuracy of about 2.5% or better. No entries appear for $X_{r||}$ since this should be infinite. In the boundary element calculations, the model structures are not perfectly axisymmetric, and consequently there is some rotational friction when the structures are rotated about the symmetry (z) axis. However, this friction decreases and goes to zero as N gets large.

As far as we are aware, this is the first time ξ has been calculated for any structure for the slip boundary case with the exception of the sphere. The BE value of 1.00 for a sphere is in excellent agreement with the prediction of Eisenschitz.[36] (Incidentally, the work of Eisenschitz appears to be largely forgotten in the modern literature.) Compared to the stick values, the slip viscosity coefficients show a weaker dependence on shape.

Rods. A large number of biopolymers have been modeled as rodlike particles, and there have been extensive numerical studies carried out of their hydrodynamic properties. Typically, they are modeled as right-circular cylinders of length L and diameter d. Broersma[50] formulated a theory of the translation and

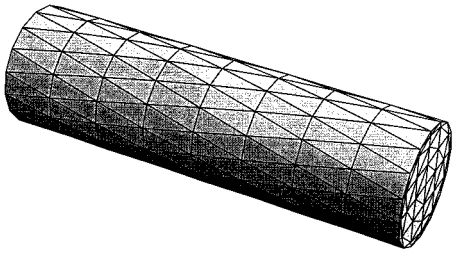

Figure 3. Representative rod model. In this example, $p = L/d = 3.4$ and $N = 384$.

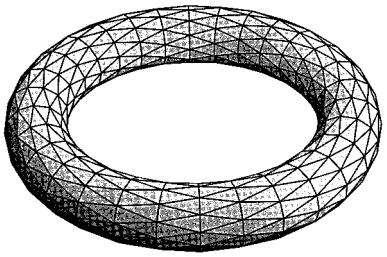

Figure 4. Representative toroid model. In this example, $p = R/r = 5.0$ and $N = 720$.

Table 3. Transport Properties of Short Cylinders

p	case	$X_{t\|\|}$	$X_{t\perp}$	X_t	$X_{r\|\|}$	$X_{r\perp}$	ξ
2.04	stick	0.978	0.869	0.904	1.16	0.518	3.43
	a	1.02	0.907	0.909	1.21	0.528	(3.16)
	slip	1.49	1.15	1.26		0.929	1.30
3.4	stick	0.951	0.786	0.839	1.28	0.317	4.60
	a	0.982	0.812	0.857	1.32	0.322	(4.55)
	slip	1.64	1.00	1.21		0.520	2.12
6.8	stick	0.859	0.650	0.719	1.39	0.134	8.70
	a	0.886	0.670	0.737	1.42	0.135	(9.05)
	b	0.656	0.563	0.549		0.122	
	slip	2.01	0.787	1.19		0.194	4.72
10.2	stick	0.786	0.569	0.642	1.44	0.0753	14.0
	a	0.807	0.581	0.654	1.47	0.0757	(14.82)
	b	0.642	0.510	0.554		0.0691	
	slip	2.25	0.672	1.20		0.103	8.35
13.6	stick	0.728	0.513	0.585	1.46	0.0491	20.5
	a	0.746	0.522	0.595	1.49	0.0490	(21.7)
	b	0.619	0.469	0.519		0.0454	
	slip	2.45	0.598	1.22		0.0646	12.5
17.0	stick	0.683	0.472	0.543	1.49	0.0348	28.0
	a	0.697	0.478	0.550	1.50	0.0346	(29.7)
	b	0.595	0.436	0.489		0.0324	
	slip	2.66	0.544	1.25		0.0444	17.4

rotation of long rods that have been extensively used in the past. More recently, the Broersma interpolation formulas have been modified to be applicable to shorter rods.[51] The claim has been made that these are valid for $p \equiv L/d > 4.6$. Garcia de la Torre and co-workers[46,52] have carried out extensive numerical studies of the translational and rotational diffusion constants of cylinders which should be valid for any value of p. In their work, the cylinders are represented as rings of beads stacked one on top of each other,[46] and transport properties are computed by an extrapolated shell procedure very similar to that employed in the present work. Also, Youngren and Acrivos[21] have carried out BE calculations of capped cylinder models translating parallel to the symmetry axis of the cylinder for the case of stick boundary conditions. The $X_{t||}$'s inferred from their work are in excellent agreement with the BE calculations of the present work. Figure 3 is a representative BE structure for a capped cylinder model employed in the present study with $p = 3.4$. A range of different structures have been modeled with p varying from 2.04 to 17.0. These correspond to models of DNA fragments with a diameter of 2.0 nm and a length range from 12 base pairs ($p = 2.04$) to 100 base pairs ($p = 17.0$). The transport properties are summarized in Table 3. The case entries marked "stick" and "slip" come from BE-extrapolated shell values determined in the present work. Also included in the table are numerical results of other investigators. The entries under "case a" for translational and rotational transport have been computed using the interpolation formulas of Garcia de la Torre and co-workers[52] which are valid for stick boundary conditions. Without exception, the present BE calculations agree with these to within a few percent. We do not claim that the results of the present study are more accurate than those of ref 52, or vice versa. As discussed in a previous subsection, accuracy of the BE-extrapolated shell procedure is limited to several percent of the actual value. Also listed under "case a" are values of the viscosity coefficient ξ. They are computed from the interpolation formulas of Yoshizaki and Yamakawa[53] for spheroid−cylinder models with stick bc's. Since their interpolation formulas are not valid for flat-ended models as employed in the present study, the entries appearing in Table 3 correspond to cylinders capped with hemispheroids which have the same total length, L, and diameter, d, as the flat-ended models. Because of differences in the two models, the "case a" entries of ξ (stick bc's) are placed in parentheses. Nonetheless, the two models are similar enough to make a qualitative comparison worthwhile. The "case b" entries represent the Broersma estimates[51] for stick bc's. These results deviate substantially from both the BE-extrapolated shell (present study), and "bead"-extrapolated shell[46,52] estimates except for very long rods. A detailed discussion of this point has already been presented.[52] To the best of our knowledge, all of the transport results on rods with slip boundary conditions are entirely new. An exact transport property is available for a long rod with stick bc's for $X_{r||}$ and equals 1.5.[54] The numerical results for $p = 17.0$ given in Table 3 are seen to be in good agreement with this.

Toroids. Although toroidal (donut)-shaped particles are not as common as rodlike particles in nature, they definitely do exist. Perhaps the best known examples are formed by the collapse of high molecular weight DNA induced by the presence of polyvalent cations under low salt conditions.[55] Translational and rotational transport coefficients are available for the stick bc case. For rotation[56] or translation[57] about the symmetry axis, results have been available for a long time. The asymmetric rotation and translation problems have been solved by Goren and O'Neill.[58] Extrapolated shell studies of translation (stick bc's) employing bead arrays have also been reported[59] and are in excellent agreement with the results of Goren and O'Neill.[58]

Figure 4 shows a representative model toroid used in the present BE studies. One can imagine generating a toroid by starting with a circle of radius "r" the center of which is at distance R from some convenient origin. The symmetry axis lies perpendicular to the line connecting the origin to the center of the circle. The toroid is then generated by rotating about the symmetry axis through 2π radians to produce a structure with volume $2\pi r^2 R$. The reduced variable, p, is defined as R/r and goes to 1.0 in the limit of toroid with vanishing inner hole. The resulting BE-extrapolated shell transport properties are summarized in Table 4 (stick and slip cases). Also included are the values of Goren and

Table 4. Transport Properties of Toroids

p	case	$X_{t\|\|}$	$X_{t\perp}$	X_t	$X_{r\|\|}$	$X_{r\perp}$	ξ
1.2	stick	0.874	0.983	0.946	0.688	0.855	2.97
	a	0.872	0.981	0.948	0.686	0.851	
	slip	1.09	1.49	1.36		2.78	1.35
2.0	stick	0.778	0.912	0.868	0.494	0.629	3.87
	a	0.776	0.910	0.866	0.493	0.624	
	slip	0.927	1.39	1.24		1.36	1.82
3.0	stick	0.686	0.828	0.781	0.338	0.430	5.37
	a	0.683	0.826	0.778	0.337	0.426	
	slip	0.794	1.26	1.11		0.731	2.70
4.0	stick	0.619	0.759	0.712	0.244	0.308	7.20
	a	0.616	0.757	0.710	0.243	0.304	
	slip	0.705	1.15	1.00		0.464	3.80
5.0	stick	0.567	0.704	0.658	0.185	0.232	9.26
	a	0.564	0.701	0.655	0.184	0.228	
	slip	0.639	1.03	0.899		0.323	5.17
6.0	stick	0.526	0.657	0.613	0.144	0.179	11.7
	a	0.523	0.655	0.611	0.144	0.177	
	slip	0.588	0.973	0.845		0.239	6.82
8.0	stick	0.465	0.586	0.546	0.0959	0.117	17.2
	a	0.463	0.584	0.544	0.0960	0.116	
	slip	0.521	0.856	0.749		0.148	10.8
10.0	stick	0.419	0.532	0.494	0.0681	0.0821	24.0
	a	0.419	0.532	0.494	0.0687	0.0822	
	slip	0.462	0.763	0.663		0.100	15.5

O'Neill[58] (case a). The stick BE-extrapolated shell translational and rotational transport properties agree with those of ref 58 to within a few percent, which is a trend consistent with that seen previously for ellipsoids and rods. To the best of our knowledge, the stick ξ values for toroids as well as all of the slip transport properties are being reported for the first time.

Discussion and Conclusion

Although the boundary element (BE) approach has been available for over 20 years and has been applied to stick[21] and slip[24] boundary condition cases, its application to problems involving slip boundary conditions has been very limited. Furthermore, the intrinsic viscosity, or the closely related reduced viscosity coefficient, ξ, is only known for a small number of geometrical models such as ellipsoids and spheroid−cylinders with stick boundary conditions. Thus, the primary motive of the present work is to fill in some gaps in our knowledge of the transport properties of some simple model structures (ellipsoids, rods, and toroids) subject to both stick and slip boundary conditions. The accuracy of the resulting transport properties is estimated to be within a few percent.

A secondary motive of the present work is to provide a stronger theoretical foundation into future studies of whether stick boundary conditions or slip or some other model[25] best describe the transport of small molecules in aqueous or nonaqueous solvents. Virtually all studies of this problem have been restricted to investigations of rotational diffusion.[22−25] In addition to slip rotational transport coefficients, we have provided slip translational transport coefficients and slip viscosity coefficients. It is hoped that these results will be useful in complementary studies of dynamic light scattering (which yields translational diffusion constants) and viscosity (which could yield ξ). Experiments that measure these are generally far easier to implement than those involved in determining rotational diffusion constants.

Acknowledgment. Professors Sergio Aragon (San Francisco State University) and Marshall Fixman (Colorado State University) deserve thanks for their comments prior to publication. Min Zhai also deserves special thanks for a literature search. We would also like to acknowledge NSF grant MCB-9807541 for partial support of this work.

References and Notes

(1) Berne, B. J.; Pecora, R. *Dynamic Light Scattering*; John Wiley & Sons: New York, 1976.
(2) Schmitz, K. S. *An Introduction to Dynamic Light Scattering by Macromolecules*; Academic Press: New York, 1990.
(3) Tao, T. *Biopolymers* **1969**, *8*, 609.
(4) Nuutero, S.; Fujimoto, B. S.; Flynn, P. F.; Reid, B. R.; Ribeiro, N. S.; Schurr, J. M. *Biopolymers* **1994**, *34*, 463.
(5) Eimer, W.; Williamson, J. R.; Boxer, S. G.; Pecora, R. *Biochemistry* **1990**, *29*, 799.
(6) Elias, J. G.; Eden, D. *Macromolecules* **1981**, *14*, 410.
(7) Stellwagen, N. C. *Biopolymers* **1981**, *20*, 434.
(8) Hagerman, P. J. *Biopolymer* **1981**, *20*, 1503.
(9) Diekmann, S.; Hillen, W.; Morgeneyer, B.; Wells, R. D.; Porschke, D. *Biophys. Chem.* **1982**, *15*, 263.
(10) Antosiewicz, J.; Porschke, D. *Biophys. Chem.* **1989**, *33*, 19.
(11) Eimer, W.; Pecora, R. *J. Chem. Phys.* **1991**, *94*, 2324.
(12) Garcia Bernal, J. M.; Garcia de la Torre, J. *Biopolymers* **1980**, *19*, 751.
(13) Laue, T. M.; Ridgeway, T. M.; Wooll, J. O.; Shepard, H. K.; Moody, T. P.; Wilson, T. J.; Chaires, J. B.; Stevenson, D. A. *J. Pharm. Sci.* **1996**, *85*, 1331.
(14) Schmitz, K. S. *Macroions in Solution and Colloidal Suspension*; VCH Publishers: New York, 1993.
(15) Ladyzhenskaya, O. A. *The Mathematical Theory of Viscous Incompressible Flow*; Gordon and Breach: New York, 1963.
(16) Batchelor, G. K. *An Introduction to Fluid Dynamics*; Cambridge University Press: Cambridge, UK, 1967.
(17) Happel, J.; Brenner, H. *Low Reynolds Number Hydrodynamics*; Martinus Nijhoff Publishers: The Hague, Netherlands, 1983.
(18) Kim, S.; Karilla, S. J. *Microhydrodynamics*; Butterworth-Heinemann: London, 1991.
(19) Einstein, A. In *Investigations on the Theory of the Brownian Movement*; Furth, R., Ed.; Cowper, A. D., Translator; Dover Publications: New York, 1956.
(20) Batchelor, G. K. *J. Fluid Mech.* **1970**, *41*, 545.
(21) Youngren, G. K.; Acrivos, A. *J. Fluid. Mech.* **1975**, *69*, 377.
(22) Hu, C.-M.; Zwanzig, R. *J. Chem. Phys.* **1974**, *60*, 4354.
(23) Bauer, D. R.; Brauman, J. I.; Pecora, R. *J. Am. Chem. Soc.* **1974**, *96*, 6840.
(24) Youngren, G. K.; Acrivos, A. *J. Chem. Phys.* **1975**, *63*, 3846.
(25) Kivelson, D. In *Rotational Dynamics of Small and Macromolecules*; Lecture Notes in Physics Vol. 293; Dorfmuller, T., Pecora, R., Eds.; Springer-Verlag: Berlin, 1987; p 1.
(26) Wolynes, P. G.; Deutch, J. M. *J. Chem. Phys.* **1976**, *65*, 450.
(27) Allison, S. A.; Nambi, P. *Macromolecules* **1992**, *25*, 3971.
(28) Allison, S. A.; Mazur, S. *Biopolymers* **1998**, *46*, 359.
(29) Booth, F. *Proc. R. Soc. London* **1950**, *A203*, 533.
(30) Sherwood, J. D. *J. Fluid Mech.* **1980**, *101*, 609.
(31) Allison, S. A. *Macromolecules* **1998**, *31*, 4464.
(32) Wegener, W. A. *Biopolymers* **1986**, *25*, 627.
(33) Allison, S. A.; Nambi, P. *Macromolecules* **1994**, *27*, 1413.
(34) IMSL User's Manual, "Math/Library Fortran Subroutines for Mathematical Applications," Houston, TX, 1987.
(35) Feynman, R. P.; Leighton, R. B.; Sands, M. In *The Feynman Lectures on Physics*; Addison-Wesley: Reading, MA, 1963; Vol. 1, Section 43-5.
(36) Eisenschitz, R. *Phys. Z.* **1933**, *34*, 411.
(37) Jeffrey, G. B. *Proc. R. Soc. London* **1923**, *A102*, 161.
(38) Simha, R. *J. Phys. Chem.* **1940**, *44*, 25.
(39) Saito, N. *J. Phys. Soc. Jpn.* **1951**, *6*, 297.
(40) van Holde, K. E. *Physical Biochemistry;* Prentice Hall: Englewood Cliffs, NJ, 1971.
(41) Cantor, C. R.; Schimmel, P. R. *Biophysical Chemistry, Part II*; W. H. Freeman: San Francisco, CA, 1980; Chapter 12.
(42) Russel, W. B. *J. Fluid Mech.* **1978**, *85*, 209.
(43) Garcia de la Torre, J.; Bloomfield, V. A. *Biopolymers* **1980**, *17*, 1605.
(44) Bloomfield, V. A.; Dalton, W. O.; van Holde, K. E. *Biopolymers* **1967**, *5*, 135.
(45) Swanson, E.; Teller, D. C.; de Haen, C. *J. Chem. Phys.* **1978**, *68*, 5097.

(46) Tirado, M. M.; Garcia de la Torre, J. *J. Chem. Phys.* **1979**, *71*, 2581.
(47) Garcia de la Torre, J.; Bloomfield, V. A. *Q. Rev. Biophys.* **1981**, *14*, 81.
(48) Perrin, F. *J. Phys. Rad.* **1936**, *7*, 1.
(49) Sutherland, W. *Philos. Mag.* **1905**, *9*, 791.
(50) Broersma, S. *J. Chem. Phys.* **1960**, *32*, 1626, 1632.
(51) Broersma, S. *J. Chem. Phys.* **1981**, *74*, 6989.
(52) Tirado, M. M.; Martinez, C. L.; Garcia de la Torre, J. *J. Chem. Phys.* **1984**, *81*, 2047.
(53) Yoshizaki, T.; Yamakawa, H. *J. Chem. Phys.* **1980**, *72*, 57.
(54) Landau, L. D.; Lifshitz, E. M. *Fluid Mechanics*; Pergamon Press: Oxford, UK, 1959; Section 18.
(55) Gosule, L. C.; Schellman, J. A. *Nature* **1976**, *259*, 333.
(56) Kanwal, R. R. *J. Fluid Mech.* **1961**, *10*, 17.
(57) Payne, L. E.; Pell, W. M. *Mathematica* **1960**, *7*, 78.
(58) Goren, S. L.; O'Neill, M. E. *J. Fluid Mech.* **1980**, *101*, 97.
(59) Allison, S. A.; Easterly, R. A.; Teller, D. C. *Biopolymers* **1980**, *19*, 1475.

MA990576C